Remote Hydrogen Plasma Chemical Vapor Deposition of Amorphous Hydrogenated Silicon–Carbon Films from an Organosilane Molecular Cluster as a Novel Single-Source Precursor: Structure, Growth Mechanism, and Properties of the Deposit

A. M. Wróbel,*,† S. Wickramanayaka, Y. Nakanishi, Y. Fukuda, and Y. Hatanaka

Research Institute of Electronics, Shizuoka University, Hamamatsu 432, Japan

Received February 16, 1995. Revised Manuscript Received April 20, 1995[⊗]

Amorphous hydrogenated silicon–carbon films (a-Si:C:H) were produced by the remote hydrogen plasma chemical vapor deposition (CVD) using tetrakis(trimethylsilyl)silane (TMSS) as a source compound. The films have been characterized by Fourier transform infrared, X-ray photoelectron, and Auger electron spectroscopies, as well as by scanning electron microscopy, ellipsometry, and contact angle measurements. The effect of substrate temperature (T_s) on the chemical structure, compositional uniformity, surface morphology, refractive index, and surface free energy of the film has been investigated. The increase in T_s involves elimination of organic moieties from the film and the formation of silicon carbide network. The films were found to be low-surface-energy and low-polar materials of an excellent morphological homogeneity exhibiting at $300 \le T_s \le 400$ °C a good compositional uniformity and stoichiometry near pure silicon carbide. The refractive index varies from 1.5 to 2.4 with rising T_s in the range 30–400 °C. On the basis of the structural data a hypothetical reaction mechanisms for the film growth and cross-linking steps have been proposed.

Introduction

The development of the remote plasma chemical vapor deposition (CVD) technique that has taken place in recent years is an important step toward the fabrication of defectless, high-quality thin-film materials. This technique, in contrast to direct plasma CVD, offers better control over growth conditions.[1] In particular, some damaging effects arising from direct interaction of the plasma and the growing film, namely, charged-particle bombardment and vacuum-ultraviolet (VUV) irradiation,[2] can be avoided.

Using biatomic gas for the plasma induction, such as hydrogen, essentially the two most important active species are generated, a monatomic (free-radical) hydrogen and VUV (121.5 nm) photons. The latter species can easily be eliminated from the reaction site by inserting a light trap to the remote section of the plasma apparatus.[3] Thereby, a homogeneous activation of the source compound, involving only hydrogen radicals, is achieved. This enables us to predict the chemistry of the deposition process, which is determined by reactivity of the source compound with hydrogen radicals. Moreover, the resulting chemical structure of the deposit is expected to be much more uniform than that of the materials produced by the direct plasma CVD. Remote hydrogen plasma CVD has been successfully used for the fabrication of various types of thin-film materials including silicon-based films: a-Si:H[3–9] and a-$Si_{1-x}N_x$:H,[10–12] as well as metal-based films: ZnSe[13] and ZnSe-S.[14]

Taking into account the mentioned beneficial features of the remote hydrogen plasma CVD, we have used this technique for the deposition of a-Si:C:H films using TMSS molecular cluster, $(Me_3Si)_4Si$, as a novel single-source precursor. An image of the molecular structure of TMSS is presented in Figure 1. The first part of this study reported previously[15] revealed a high reactivity of TMSS with hydrogen radicals which is attributed to

† Polish Academy of Sciences, Centre of Molecular and Macromolecular Studies, Sienkiewicza 112, 90-363 Łódź, Poland.
⊗ Abstract published in *Advance ACS Abstracts*, June 1, 1995.

(1) Lucovsky, G; Tsu, D. V.; Rudder, R. A.; Markunas, R. J. In *Thin Film Processes II*; Vossen, J. L., Kern, W., Eds.; Academic Press: Boston, MA, 1991; Chapter 4.
(2) Wróbel, A. M.; Czeremuszkin, G. *Thin Solid Films* **1992**, *216*, 203.
(3) Meikle, S.; Nakanishi, Y.; Hatanaka, Y. *J. Vac. Sci. Technol.* **1991**, *A9*, 1051.
(4) Johnson, N. M.; Walker, J.; Doland, C. M.; Winer, K.; Street, R. A. *Appl. Phys. Lett.* **1989**, *54*, 1872.
(5) Johnson, N. M.; Nebel, C. E.; Santos, P. V.; Jackson, W. B.; Street, R. A.; Stevens, K. S.; Walker, J. *Appl. Phys. Lett.* **1991**, *59*, 1443.
(6) Meikle, S.; Nakanishi, Y; Hatanaka, Y. *Jpn. J. Appl. Phys.* **1990**, *29*, L2130.
(7) Kuroiwa, K.; Yamazaki, H.; Tsuchiya, S.; Kamisako, K.; Tarui, Y. *Jpn. J. Appl. Phys.* **1992**, *31*, L518.
(8) Shaw, D. M.; Sheng, T.; Yu, Z.; Collins, G. J.; Adachi, N. *Jpn. J. Appl. Phys.* **1992**, *31*, 3515.
(9) Yoshida, A.; Inoue, K.; Ohashi, H.; Saito, Y. *Appl. Phys. Lett.* **1990**, *57*, 484.
(10) Ueno, T.; Nagayoshi, H.; Morinaka, H.; Kuroiwa, K.; Tarui, Y. *Jpn. J. Appl. Phys.* **1992**, *31*, 3972.
(11) Yasui, K.; Nasu, M.; Komaki, K.; Kaneda, S. *Jpn. J. Appl. Phys.* **1990**, *29*, 918.
(12) Yasui, K.; Nasu, M.; Kaneda, S. *Jpn. J. Appl. Phys.* **1990**, *29*, 2822.
(13) Oda, S.; Kawase, R.; Sato, T.; Shimizu, I.; Kokado, H. *Appl. Phys. Lett.* **1986**, *46*, 33.
(14) Fujiwara, H.; Gotoh, J.; Shirai, H.; Shimizu, I. *J. Appl. Phys.* **1993**, *74*, 5510.

0897-4756/95/2807-1403$09.00/0 © 1995 American Chemical Society

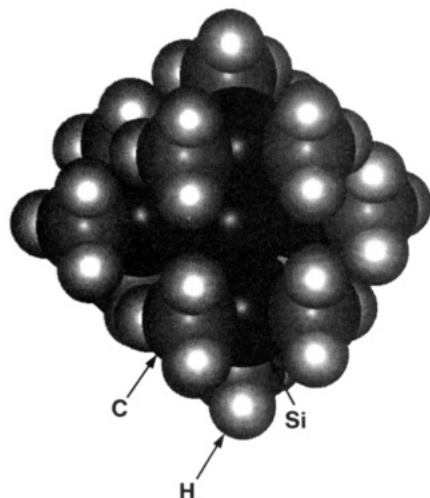

Figure 1. Image of tetrakis(trimethylsilyl)silane molecule, 1.07 nm in a mean size.

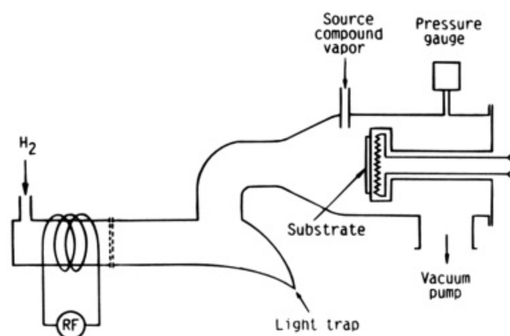

Figure 2. Schematic diagram of the remote plasma CVD apparatus.

the presence of four Si–Si bonds in a tetrahedral molecular skeleton. This is well illustrated by the results of a comparative deposition experiments which showed that the deposition rate for TMSS was higher than that of hexamethyldisilane and teramethylsilane source compounds, by about 3 and 30 times, respectively.[15] Owing to a high reactivity and the relatively low atomic ratio of carbon to silicon in the molecular structure of TMSS (C/Si = 2.4), this compound is an attractive precursor for the a-Si:C:H films.

The present paper reports the results of structural study of thin-film materials produced from TMSS by the remote hydrogen plasma CVD, which were obtained using various spectroscopic methods. The effect of substrate temperature (or deposition temperature) on chemical structure, compositional uniformity, surface morphology, as well as optical and surface energy properties of the deposit is discussed. On the basis of the structural study a hypothetical mechanisms of the elementary reactions contributing to the film growth are postulated.

Experimental Section

The remote plasma CVD apparatus used for the present study is shown in Figure 2. The apparatus consisted of two major parts: (1) plasma generation tube of 31 mm i.d. (made of fused silica) with a coil coupled via a matching network with a radio frequency (13.56 MHz) power supply unit; (2) an afterglow tube (made of Pyrex glass) expanded to 78 mm i.d. in the deposition section which contained the substrate holder equipped with a heater and a temperature control unit. A source compound injector (4 mm i.d.) was located approximately 8 cm in front of the substrate holder. To prevent VUV irradiation of the film during growth, a Wood's horn light trap was inserted into the afterglow tube before the deposition section. The distance between the plasma edge and substrate was about 25 cm. Films were deposited on p-type c-Si wafers (⟨111⟩ orientation, resistivity 90–100 Ω cm, and surface area approximately 9 cm^2) under following conditions: total pressure $p = 0.2$ Torr (27 Pa), hydrogen flow rate $F(H_2) = 200$ sccm, rf power input $P = 200$ W, and substrate temperature $T_s = 30–400$ °C.

TMSS source compound (STREM Chemicals product, 99% purity, mp 262 °C) was evaporated at the temperature of 80 °C in argon flowing through the evaporator with the rate $F(Ar)=1$ sccm and fed to the reactor with the flow rate $F(TMSS) = 0.5$ sccm.

Film thickness and refractive index were measured ellipsometrically using a Nippon Infrared Industrial Co. EL-101D ellipsometer. For each sample the average thickness and refractive index values were calculated from at least five ellipsometrical measurements. The thickness of the film samples deposited in the present study ranges from about 200 to 500 nm.

Fourier transform infrared (FTIR) transmission spectra of the films deposited on c-Si wafers were run on a Horiba FT-300A spectrophotometer. Raman spectroscopic analyses were performed using a Jobin Yvon Ramanor HG2S spectrophotometer.

X-ray photoelectron spectra (XPS) were run on an ULVAC PHI 510 surface analysis instrument using Mg Kα X-rays as the photoexcitation source with an electron takeoff angle of 45° from the surface normal. Prior to analysis the surface of the film sample was cleaned by sputter etching with a 1 kV Ar^+ beam for 15 min. Curve fitting with mixed Gaussian/Lorentzian functions was performed on unsmoothed data following background substraction.

Auger electron spectroscopic (AES) analysis was performed using an ULVAC AQM 808 system. Compositional AES depth profiling was carried out by sputter-etching of the film sample with a 2 kV Ar^+ beam.

The morphology of film surface was examined by scanning electron microscopy (SEM) using a JEOL JSM 6100 electron microscope. Surface wettability of the films was characterized by measuring the advancing contact angle of sessile drops of five test liquids: water, glycerol, formamide, ethylene glycol, and tricresyl phosphate.

The contact angle was measured at room temperature with an Erma G-1 microscopic goniometer. For each liquid an average of 5–10 readings was calculated. The contact-angle data were then evaluated to determine dispersion and polar components of the surface energy according to a model for low-energy surfaces developed by Kaelble.[16]

Results and Discussion

Reaction System. Our earlier study[15] of the activation of TMSS in remote hydrogen plasma CVD allows to characterize the reaction system. To estimate the mass flow regime in the remote part of the apparatus the Peclect number $Pe = vL/D$ (where v is the average flow velocity of hydrogen, L is the distance between the plasma edge and the substrate, and D the diffusivity of the source compound) has been evaluated. This number, being the ratio of convection to diffusion, is useful for assessing the importance of back diffusion of the source compound molecules. For the present experimental conditions, hydrogen concentration, and temperature data given below has been calculated $v = 1.9$

(15) Wróbel, A. M.; Wickramanayaka, S.; Hatanaka, Y. *J. Appl. Phys.* **1994**, *76*, 558.

(16) Kaelble, D. H. *Physical Chemistry of Adhesion*; Wiley-Interscience: New York, 1971; Chapter 5.

$\times 10^3$ cm s^{-1}. Assuming the mean size of TMSS molecule as 1.07 nm (the value has been computed using HyperChem v.4.0 for Windows software) we evaluated $D < 10^3$ cm^2 s^{-1}. Taking into account these data and $L = 25$ cm we found $Pe \gg 10$. This value of Pe indicates that the diffusion of the source compound to the plasma section can be neglected,[17] and thus the activation of TMSS molecules exclusively takes place in the deposition section. Moreover, the zero value of thermal activation energy found from the Arrhenius plot of the substrate temperature dependence of the deposition rate suggests that the activation step proceeds in the gas phase and the deposition process is controlled by the diffusion of the film-forming species from the gas phase to the substrate.[15] Concentration of the atomic hydrogen in the reactor determined by the NO_2 titration method[15] is [H] = 5.1×10^{15} cm^{-3}. Using this value and total concentration of the gas molecules in the reactor (under the pressure of 0.2 Torr and at the estimated temperature of 306 K) as [G] = 6.4×10^{15} cm^{-3}, we find the fraction of hydrogen atoms at the reaction site to be f_H = [H]/[G] = 0.79.[15] On the basis of the latter value and the flow rate data of the reagents, we have evaluated the approximate number of hydrogen radicals per molecule of the source compound as $N_H = f_H F(H_2)/F(\text{TMSS}) = 3 \times 10^2$ atoms/molecule.

Chemical Structure of the Deposit. *Fourier transform infrared and Raman spectroscopies:* The FTIR transmission spectra of the films deposited at various substrate temperatures are shown in Figure 3 which also presents, for comparison, the spectrum of TMSS source compound. The most important absorption bands and their assignments based on the literature IR data[18,19] are listed in Table 1. As can be noted from Figure 3, film spectra b−e reveal the presence of a strong absorption band with a maximum in the range 1010−980 cm^{-1} characteristic of carbosilane Si−CH_2−Si units, and weak intensity band at 2160 cm^{-1} from SiH_x groups, which are absent from the TMSS spectrum (Figure 3a). The former band may be interfered with the absorption arising from Si−O−Si and/or Si−O−C linkages, which also falls in this region. A further important observation is that a distinct band from Si−Si bonds present in the spectrum of TMSS at 455 cm^{-1} does not appear in the film spectra. These data bear a witness of an intense decomposition of Si−Me and Si−Si units in TMSS molecules and following formation of chemically more stable Si−CH_2−Si linkages in the deposit.

The increase in the substrate temperature involves substantial changes in the film spectra. A drop of the absorption in the range 1260−1240 cm^{-1}, from $SiMe_x$, to the zero value for $T_s \geq 300$ °C (Figure 3e,f) is observed. This is due to thermal scission of the Si−C bonds in methylsilyl groups. Moreover, a marked increase of the absorption in the range 830−800 cm^{-1}, attributed to the Si-C carbidic units,[20−22] with respect to the intensity of the band in 1010−980 cm^{-1} region, arising from Si−CH_2−Si, is noted. The latter change is associated with thermally assisted conversion of the Si−CH_2−Si linkages into carbosilane units with tertiary and quaternary carbon, i.e., Si_3CH and Si_4C, respectively. In view of the FTIR spectroscopic data the increase of the substrate temperature eliminates organic moieties incorporated to the film from the source compound and leads to the formation of Si−C carbidic network in the deposit.

The most important information provided by the Raman spectroscopy is that a distinct band with a

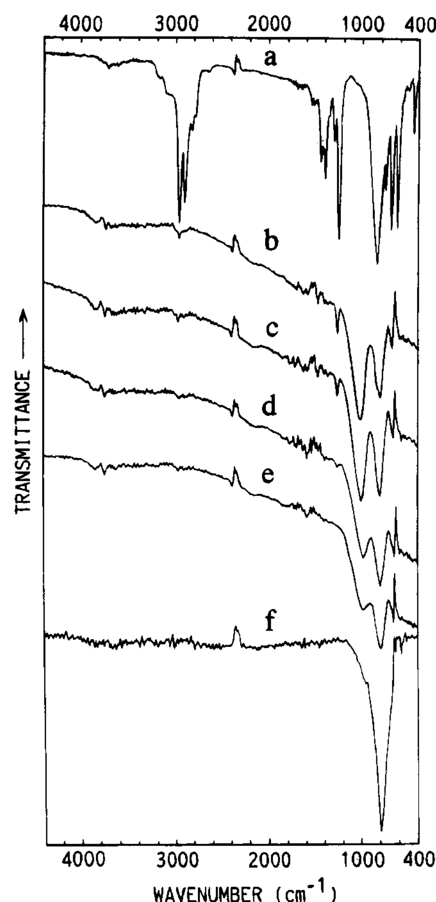

Figure 3. FTIR transmission spectra of TMSS source compound in KBr pellet (a) and the films deposited on c-Si wafer at various temperatures T_s: 30 (b), 90 (c), 200 (d), 300 (e), and 400 °C (f).

Table 1. Infrared Absorption Bands Detected in the Transmission FTIR Spectra of TMSS Source Compound and Its Films Deposited at the Substrate Temperature T_s = 30−400 °C

absorption band (cm^{-1})	TMSS spectrum	film spectra[a]	assignment
2960−2950	+	+ (T_s < 300 °C)	C−H asym str
2910−2890	+	+ (T_s < 300 °C)	C−H sym str
2160	−	+	Si−H str in SiH_x
1260−1240	+	+ (T_s < 300 °C)	−CH_3 sym def in $Si(CH_3)_x$
1010−980	−	+	−CH_2− wagging in Si−CH_2−Si; Si−O−Si and/or Si−O−C str
830−800	+	+	Si−C str
455	+	−	Si−Si asym str

[a] +, presence; −, absence.

(17) Jensen, K. F. In *Chemical Vapor Deposition. Principles and Application*; Hitchman, M. L., Jensen, K. F., Eds.; Academic Press: London, 1993; Chapter 2, pp 53−56.
(18) Anderson, D. R. In *Analysis of Silicones*; Smith, A. L., Ed.; Wiley-Interscience: New York, 1974; Chapter 10.
(19) Lipp, E. D.; Smith, A. L. In *The Analytical Chemistry of Silicones*; Smith, A. L., Ed.; Wiley-Interscience: New York, 1991; Chapter 11.
(20) Tsai, H. K.; Lin, W. L.; Sah, W. J.; Lee, S. C. *J. Appl. Phys.* **1988**, *64*, 1910.
(21) Bhusari, D. M.; Kshirsagar, S. T. *J. Appl. Phys.* **1993**, *73*, 1743.
(22) Delplancke, M. P.; Powers, J. M.; Vandentop, G. J.; Salmeron, M.; Somorjai, G. A. *J. Vac. Sci. Technol.* **1990**, *A9*, 450.

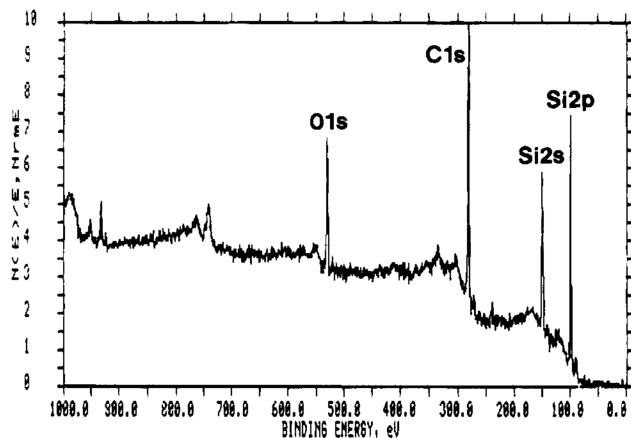

Figure 4. XPS spectrum of the film deposited on c-Si wafer at the temperature T_s = 30 °C and subjected to cleaning by Ar^+ sputter etching.

maximum at 456 cm^{-1} present in the spectrum of TMSS, and originating from the asymmetric stretching mode of the Si-Si[18] has not been detected in the spectra of the films, regardless of the deposition temperature, thus accounting for the absence of these units in the deposit.

X-ray Photoelectron Spectroscopy. The XPS spectrum typical of the deposited films is shown in Figure 4. The spectrum reveals the presence of distinct peaks originating from Si2p, Si2s, C1s, and O1s core levels. The high-resolution spectra in these regions (except Si2s core-level) are presented in Figure 5, which shows that the Si2p, C1s, and O1s spectral envelopes are resolved into four silicon, three carbon, and three oxygen peaks, respectively. The assignment of the particular peaks in these spectra was based on the XPS literature data referring to the a-Si:C:H[22-29] and a-Si:H[30] films produced by various CVD techniques. The XPS examination was performed for the films deposited at various substrate temperatures in the range 30−400 °C, and the XPS data are summarized in Table 2, which specifies the peak binding energy and the full width at half-maximum (fwhm) mean values, as well as the peak origins. The detected peak binding energies in Table 2 may somewhat differ from the real values. This is evident in the case of peak 2 in the C1s envelope (Figure 5), which originates from the aliphatic carbon. The binding energy observed for this peak, 284.0 eV (Table 2), differs by about 1 eV from the real value, 285.0 eV, which usually is a reliable reference. Similar shifts in binding energies we have also noted in the XPS spectra of the a-Si:C:H films produced from $C_2H_4/SiH_4/H_2$ source mixture by the direct plasma CVD.[24]

The XPS spectra in Figure 5 and identification data in Table 2 provide an important information regarding structure of the film deposited onto unheated substrate. The high-intensity peaks observed in the Si2p spectrum at 101.1 eV (peak 2) and 102.2 eV (peak 3) account for

(23) Hicks, S. E.; Fitzgerald, A. G.; Baker, S. H.; Dines, T. J. *Philos. Mag.* **1990**, *B62*, 193.
(24) Suzuki, Y.; Meikle, S.; Fukuda, Y.; Hatanaka, Y. *Jpn. J. Appl. Phys.* **1990**, *29*, L663.
(25) Tabata, A.; Fujii, S.; Suzoki, Y.; Mizutani, T.; Ieda, M. *J. Phys. D: Appl. Phys.* **1990**, *23*, 316.
(26) Chiu, H. T.; Lee, S. F. *J. Mater. Sci. Lett.* **1991**, *10*, 1323.
(27) Favia, P.; Fracassi, F.; d'Agostino, R. *J. Biomater. Sci. Polym. Ed.* **1992**, *4*, 61.
(28) Takeshita, T.; Kurata, Y.; Hasegawa, S. *J. Appl. Phys.* **1992**, *71*, 5395.
(29) Suzuki, H.; Araki, H.; Noda, T. *Jpn. J. Appl. Phys.* **1993**, *32*, 3566.
(30) Kawasaki, M.; Suzuki, H. *J. Appl. Phys.* **1994**, *75*, 3456.

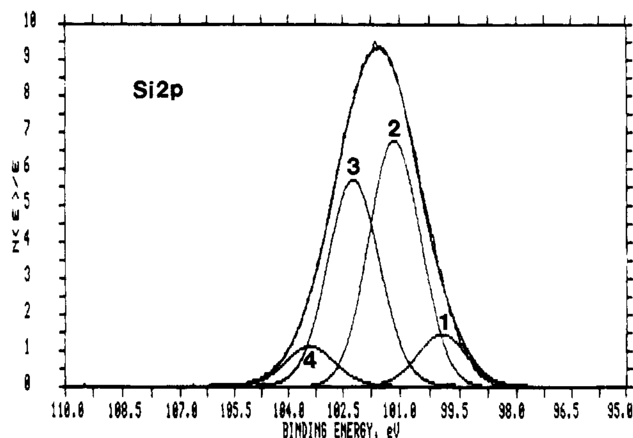

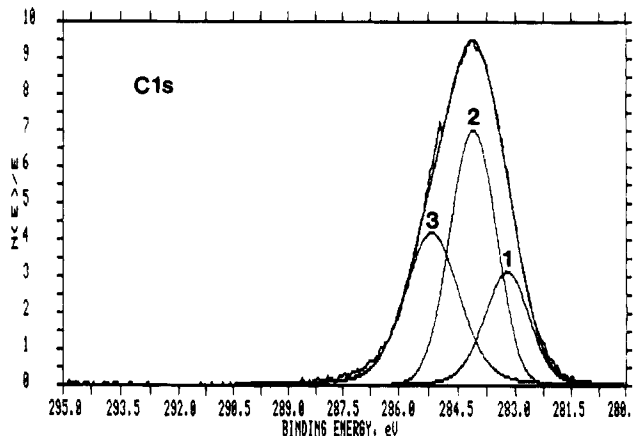

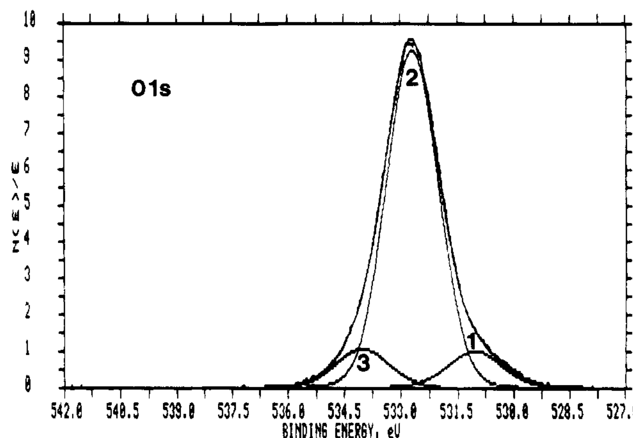

Figure 5. XPS spectra of Si2p, C1s, and O1s core-levels of the film deposited at the substrate temperature T_s = 30 °C.

Table 2. XPS Core Level Data for the Films Deposited from TMSS at the Substrate Temperature T_s = 30−400 °C

core level	peak no.	binding energy (eV)	fwhm (eV)	origin
Si(2p)	1	99.8 ± 0.3	1.6	Si−H, Si−Si
	2	101.1 ± 0.2	1.6	Si−C (carbidic)
	3	102.2 ± 0.2	1.7	Si−CH_x (x = 1−3)
	4	103.2 ± 0.2	1.7	Si−O
C(1s)	1	283.1 ± 0.1	1.5	C−Si
	2	284.0 ± 0.2	1.5	CH_x (x = 1−3), C−C
	3	285.0 ± 0.1	1.6	C−O
O(1s)	1	531.3 ± 0.3	1.7	C−O−H
	2	532.5 ± 0.2	1.7	O−C
	3	534.0 ± 0.2	1.7	O−Si

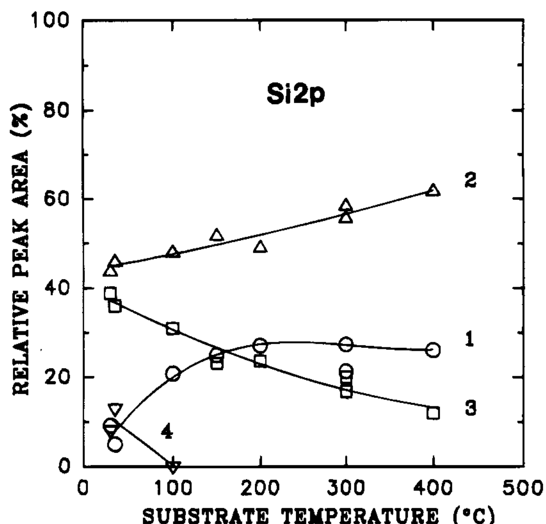

Figure 6. Relative intensity of the particular peaks in the Si2p envelope, corresponding to various silicon bonding: (1) Si–H and/or Si–Si, (2) Si–C carbidic, (3) Si–CH_x, and (4) Si–O, as a function of the substrate temperature.

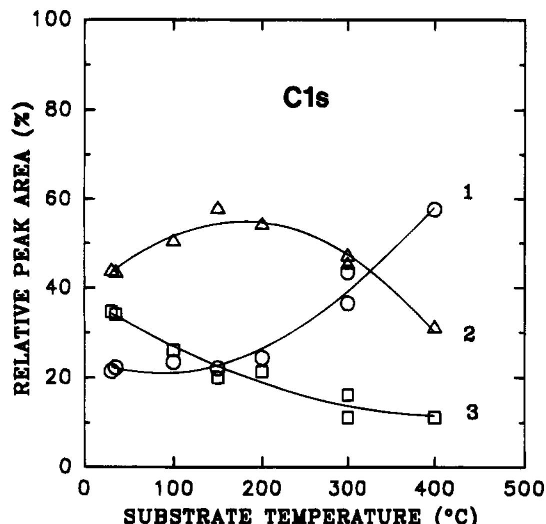

Figure 7. Relative intensity of the particular peaks in the C1s envelope, corresponding to various carbon bonding: (1) C–Si, (2) CH_x, and (3) C–O, as a function of the substrate temperature.

a large content of the Si–C carbidic and Si–CH_x units, respectively. The low-intensity peaks at 99.8 eV (peak 1) and 103.2 eV (peak 4) are assigned to the Si–H and/or Si–Si and Si–O units, respectively. According to the Raman spectroscopic data discussed in the previous section, peak 1 seems to arise from the Si–H rather than from the Si–Si units. The C1s spectrum (Figure 5) reveals an intense signal at 284.0 eV (peak 2) which is assumed to originate predominantly from the CH_x units, and the medium-intensity signals, at 283.1 (peak 1) and 285.0 eV (peak 3), ascribed to the C–Si and C–O bonds, respectively. In the O1s spectrum (Figure 5) the intensity of peak 2 at 532.5 eV characteristic of the O–C units, predominates. Two other peaks, but of weak intensity, at 531.3 (peak 1) and 534.0 eV (peak 3), are also observed in this spectrum. Peak 1 corresponds to the hydroxyl group bonded to carbon (C–O–H unit) whereas peak 3 originates from the O–Si units.

We assume that the presence of the oxygen-containing units in the deposit, as proved by the XPS spectra in Figure 5, is associated with two potential oxygen sources. The first source may be the etching of the silica wall in the plasma section with atomic hydrogen and resulting incorporation of the oxygen-containing etching products into the growing film. The second source are presumably reactions of the dangling bonds present in the deposit with the atmospheric oxygen or moisture, which may occur after the film exposure to the ambient.

The effect of the substrate temperature on the structure of the deposit examined by the XPS, is illustrated in Figures 6–8 which show the relative intensity of the particular peaks in the Si2p, C1s, and O1s core-level spectra (expressed by the ratio of the peak area to its envelope area) in Figure 5, as a function of T_s. From data in Figure 6 representing the intensity curves of the Si2p peaks it is evident that the increase of T_s gives rise to the concentration of Si–C carbidic units (curve 2) while the contents of Si–CH_x (curve 3) and Si–O (curve 4) are seen to decrease. Curve 1 demonstrates some rise of the content of Si–Si and/or Si–H units which gains a constant level for $T_s \geq 150$ °C.

The C1s intensity data in Figure 7 reveal a marked increase in the concentration of C–Si units (curve 1)

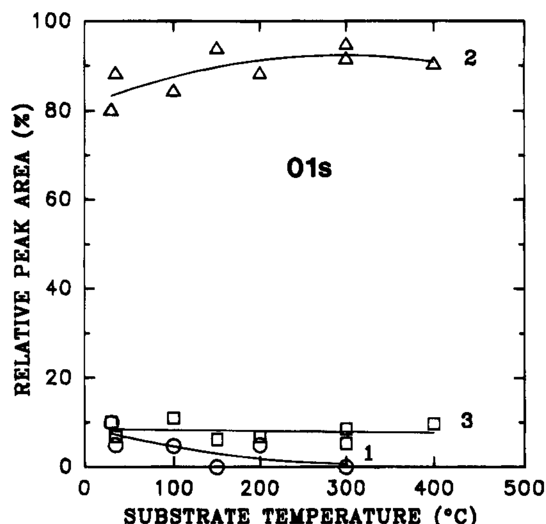

Figure 8. Relative intensity of the particular peaks in the O1s envelope, corresponding to various oxygen bonding: (1) C–O–H, (2) O–C, and (3) O–Si, as a function of the substrate temperature.

for $T_s > 200$ °C. The content of CH_x groups illustrated by curve 2, reaches a maximum value at $T_s = 150$ °C. The rise in the curve 2 noted for $T_s \leq 150$ °C is associated with increasing contribution of carbosilane Si–CH_2–Si units in the deposit that takes place in this range of T_s. In the light of the FTIR data in Figure 3 the formation of these units appears to be the major process in the film growth step at low-deposition temperatures. The drop in this curve observed for $T_s \geq 150$ °C is due to thermally induced cross-linking process involved in the dehydrogenation of the Si–CH_2–Si units and resulting formation of the Si–C carbidic network, as indicated in the previous section. The curve 3 in Figure 7 accounts for the drop in the concentration of C–O units with increasing T_s.

Inspecting the O1s intensity data in Figure 8, one may note from curve 1 that the increase of T_s up to 300 °C involves the elimination of the C–OH groups from the deposit. Curve 2 shows the content of the O–C units to increase very slightly with T_s, whereas the contribution of the O–Si units, according to curve 3,

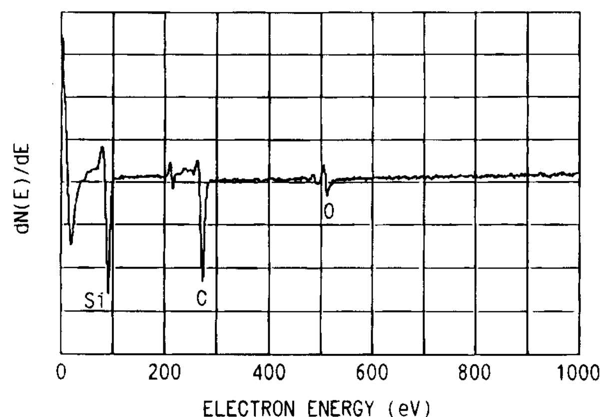

Figure 9. AES spectrum of surface of the film deposited on c-Si wafer at the temperature T_s = 100 °C.

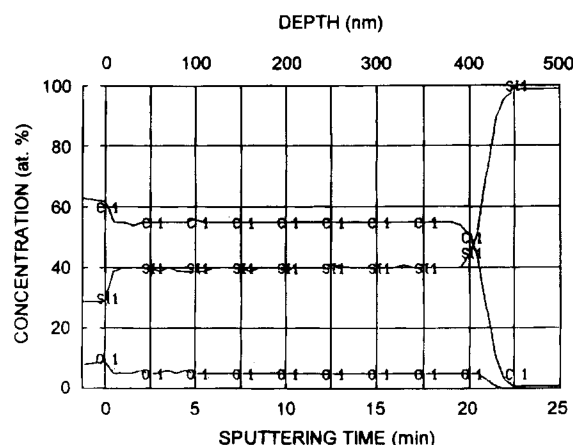

Figure 10. AES compositional depth profile of the film deposited on c-Si wafer at the temperature T_s = 100 °C.

remains at the constant level, regardless of the substrate temperature.

The trends observed in the XPS peak intensity curves in Figures 6–8 are generally consistent with the FTIR data (Figure 3) and prove that in the case of high-substrate-temperature deposit the Si–C carbidic bonds predominate in the structure of this material. The presence of the oxygen-containing units is also detected.

Auger Electron Spectroscopy. The AES spectrum representative of the deposited films is shown in Figure 9. The spectrum exhibits high-intensity peaks at 92 and 275 eV, characteristic of silicon Si(LVV) and carbon C(KLL), respectively, as well as the low-intensity peak at 512 eV originating from oxygen O(KVV).[31] To examine the compositional uniformity of the films the AES depth profiling was performed for the materials produced at various substrate temperatures. A typical compositional AES depth profile presenting a variation of the atomic concentrations of silicon, carbon, and oxygen with the film depth is illustrated in Figure 10. It is apparent from the data in this figure that the concentrations of particular elements, except for the film surface and film/substrate interface regions, remain constant independently of the depth, thus revealing an excellent copositional uniformity of the deposit, which seems to be better than that of a-Si:C:H films produced from an organosilicon source compounds by the direct

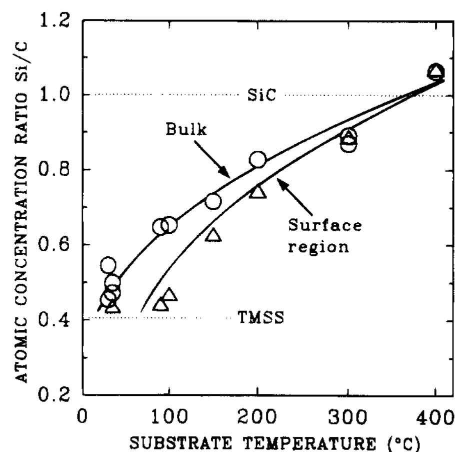

Figure 11. AES atomic concentration ratio Si/C determined for the film surface region (Δ) and the bulk at the depth of 100 nm (○), as a function of the substrate temperature.

plasma CVD.[32,33] The constant level of oxygen throughout the film depth (6 at. %) as noted in Figure 10, suggests that this element is predominantly uptaken during the film growth and its main source is the etching of silica tube with hydrogen plasma. The oxygen content in the bulk of the deposit was found to drop to 1–3 at. % with rising T_s to 300–350 °C.

The effect of the substrate temperature on the composition and compositional uniformity of the film is shown in Figure 11 which presents the AES atomic concentration ratio Si/C determined for the surface region (after sputter etching of the film with 2 kV Ar^+ beam for 2 min) and the bulk (at the depth of 100 nm) as a function of T_s. The dotted lines marked at Si/C = 0.42 and 1.0 correspond to the stoichiometry of TMSS source compound and pure silicon carbide, respectively. As can be noted in Figure 11 the ratio Si/C for the film surface region and the bulk increases with rising substrate temperature and at $T_s \approx 350$ °C reaches a value close to 1.0, which corresponds to that of pure silicon carbide. Furthermore, the data in Figure 11 prove that the difference in the stoichiometry of the surface region and the bulk is diminishing with increasing T_s. The films produced at $T_s \geq 300$ °C display a good compositional uniformity which is revealed by the same values of the atomic ratio Si/C found for the surface region and the bulk.

Mechanism of the Film Growth

Actvation Step. To estimate the susceptibility of particular bonds in the TMSS molecule toward the reaction with hydrogen radicals, we performed the deposition experiments using methane, tetramethylsilane (TMS), and hexamethyldisilane (HMDS) as the model source compounds which simulate the C–H, Si–C, and Si–Si bonds, respectively. To avoid an undesirable effect which might arise from the thermochemical reactions, the experiments were carried out with an unheated substrate. The reactivity of these compounds in the remote hydrogen plasma CVD was analyzed by the yield of the deposition, *R/FM*, where *R* is the deposition rate, *F* is the volumetric flow rate of the

(31) Davis, L. E.; MacDonald, N. C.; Palmberg, P. W.; Riach, G. E.; Weber, R. E. *Handbook of Auger Electron Spectroscopy*; Physical Electronic Ind., Inc.: Eden Prairie, MN, 1978.

(32) Loboda, M. J.; Baumann, S.; Edgell, M. J.; Stolt, K. *J. Vac. Sci. Technol.* **1992**, *A10*, 3532.

(33) Maya, L. *J. Vac. Sci. Technol.* **1994**, *A12*, 754.

source compound vapor, and M is the molecular weight of the source compound. The composite parameter R/FM expresses the thickness or mass of the deposit per unit mass of the source compound fed to the reactor and was found to be very sensitive to the molecular structure of the compound.[34,35] It is noteworthy that the deposition yield parameter has successfully been used in our recent study[36] for the determination of reactivity of such organosilicon source compounds as TMS, 1,1,1,3,3-pentamethyldisilamethane, and 1,1,3,3-tetramethyl-1,3-disilacyclobutane in the direct plasma CVD.

The values of the deposition rate determined for the examined model compounds and the calculated deposition yields are listed in Table 3, which, for comparison also contains respective data for the TMSS. The zero value of the deposition rate observed for methane accounts for the inactivity of the C–H bonds in the investigated activation step. The very close values of R/FM found for HMDS and TMSS (Table 3) which, on the other hand, are higher than that of TMS by more than one order of magnitude, prove that the Si–Si bonds play a predominant role in the activation of TMSS. The contributions of particular bonds in the TMSS to the activation step, evaluated from the deposition yield data in Table 1, are 0% for C–H, 7% for Si–C, and 93% for Si–Si. These results account for a high selectivity of the activation of source compound in the examined remote plasma CVD.

On the basis of these results and some literature data[37] reporting the gas-phase reactions of hydrogen radicals with organosilanes, we postulate a hypothetical mechanism of the activation of TMSS in the investigated remote hydrogen plasma CVD process. The primary reactions involved in this mechanism may proceed mostly by attachment of the hydrogen radical to the silicon atom either in the trimethylsilyl group or in a central position. Then the abstraction of tris(trimethylsilyl)silyl and trimethylsilyl radicals follows as shown below:

$$H^{\bullet} + (Me_3Si)_4Si \rightarrow Me_3SiH + (Me_3Si)_3Si^{\bullet} \quad (1)$$

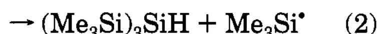

$$\rightarrow (Me_3Si)_3SiH + Me_3Si^{\bullet} \quad (2)$$

Reaction 1 is statistically favored, since there are four available sites for Si–Si bond cleavage to occur in the TMSS molecule. The radical structures produced in reactions 1 and 2 may undergo secondary reaction with TMSS:

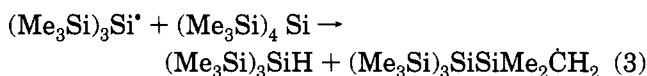

$$(Me_3Si)_3Si^{\bullet} + (Me_3Si)_4Si \rightarrow (Me_3Si)_3SiH + (Me_3Si)_3SiSiMe_2\dot{C}H_2 \quad (3)$$

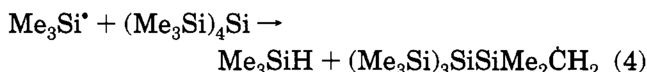

$$Me_3Si^{\bullet} + (Me_3Si)_4Si \rightarrow Me_3SiH + (Me_3Si)_3SiSiMe_2\dot{C}H_2 \quad (4)$$

The radical product of reactions 3 and 4 may isomerize and subsequently dissociate to tris(trimethylsilyl)silyl radical and dimethylsilene:[38,39]

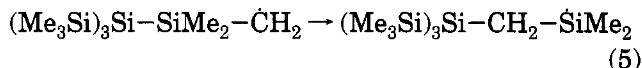

$$(Me_3Si)_3Si{-}SiMe_2{-}\dot{C}H_2 \rightarrow (Me_3Si)_3Si{-}CH_2{-}\dot{S}iMe_2 \quad (5)$$

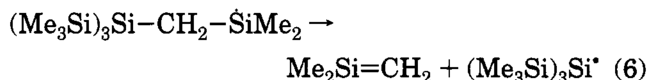

$$(Me_3Si)_3Si{-}CH_2{-}\dot{S}iMe_2 \rightarrow Me_2Si{=}CH_2 + (Me_3Si)_3Si^{\bullet} \quad (6)$$

Reactions 5 and 6 are endothermic,[38,39] and therefore they may easily proceed on a heated substrate. Trimethylsilyl radicals formed via reaction 2 may undergo disproportionation due to a relatively high value of the gas-phase disproportionation to combination rate constants ratio, which was found to be 0.5:[40,41]

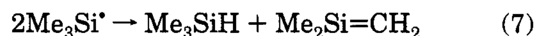

$$2Me_3Si^{\bullet} \rightarrow Me_3SiH + Me_2Si{=}CH_2 \quad (7)$$

We assume that dimethylsilene is the most important film-forming precursor which play a vital role in the growth step.

Growth Step. In light of the presented structural data we propose a hypothetical mechanisms of the elementary reactions contributing to the film growth. Dimethylsilene formed in the activation step may propagate the growth of linear carbosilane segments by the insertion to the Si–Me bonds[38,39] in the TMSS molecules adsorbed on the substrate, according to the stepwise process described by reaction 8:

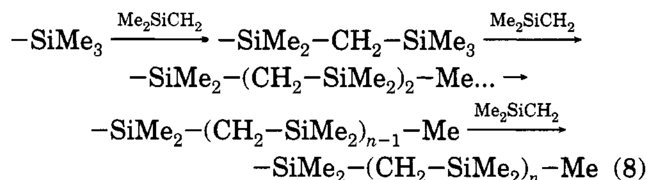

$$-SiMe_3 \xrightarrow{Me_2SiCH_2} -SiMe_2{-}CH_2{-}SiMe_3 \xrightarrow{Me_2SiCH_2} -SiMe_2{-}(CH_2{-}SiMe_2)_2{-}Me... \rightarrow -SiMe_2{-}(CH_2{-}SiMe_2)_{n-1}{-}Me \xrightarrow{Me_2SiCH_2} -SiMe_2{-}(CH_2{-}SiMe_2)_n{-}Me \quad (8)$$

Branching the linear segments via analogous insertion reaction may also take place (reaction 9):

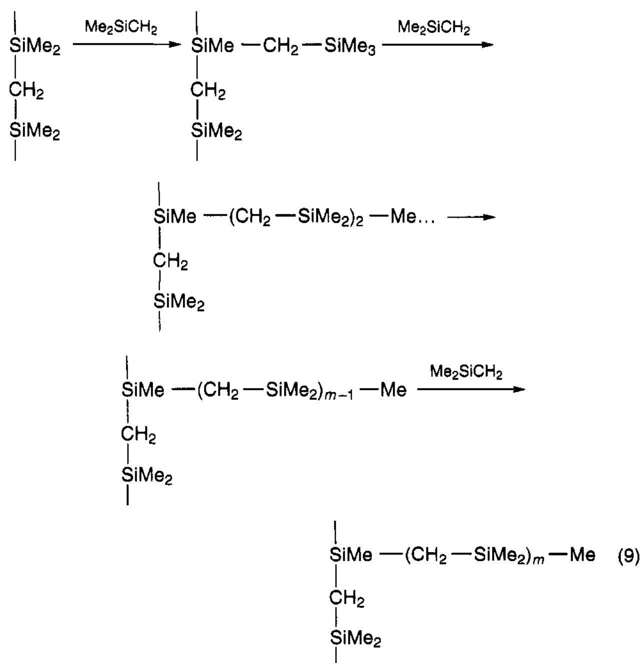

(34) Yasuda, H. *Plasma Polymerization*; Academic Press: Orlando, FL, 1985; Chapter 6, pp 169–171.
(35) Sharma, A. K. *J. Polym. Sci., Part A, Polym. Chem. Ed.* **1986**, *24*, 3077.
(36) Wróbel, A. M.; Stańczyk, W. *Chem. Mater.* **1994**, *6*, 1766.
(37) Ellul, R.; Potzinger, P; Reiman, B. *J. Phys. Chem.* **1984**, *88*, 2793.
(38) Raabe G.; Michl, *J. Chem. Rev.* **1986**, *85*, 419.
(39) Fritz, G.; Matern, E. *Carbosilanes*; Springer-Verlag: Berlin, 1986; Chapter 2.
(40) Tokach, K; Koob, R. D. *J. Phys. Chem.* **1979**, *83*, 774.
(41) Tokach, S. K.; Koob, R. D. *J. Am. Chem. Soc.* **1980**, *102*, 376.

Table 3. Yield of the Deposition Process (*R/FM*) Determined for the Model Compounds Simulating Particular Bonds in Tetrakis(trimethylsilyl)silane, at the Following Deposition Conditions: p = 0.2 Torr, $F(H_2)$ = 200 sccm, P(rf) = 200 W, and T_s = 30–35 °C

bond	model compound	mol wt M (g mol^{-1})	flow rate F (sccm)	deposition rate R (nm min^{-1})	deposition yield $R/FM \times 22.4 \times 10^2$ (nm g^{-1})
C–H	CH_4	16	8.0	0	0
Si–C	$SiMe_4$	88	1.0	0.2	5
Si–Si	$(Me_3Si)_2$	146	0.4	2.0	77
	$(Me_3Si)_4Si$	321	0.5	5.4	75

Reactions 8 and 9 predominate at low substrate temperatures and are consistent with the presence in the FTIR spectra of the films deposited at $30 \le T_s \le 90$ °C (Figure 3b,c), a very strong absorption band with a maximum in the range 1010–980 cm^{-1} which mostly originates from the Si–CH_2–Si units. Furthermore, the reactions account for the increase in the concentration of the CH_x groups as follows from the XPS C1s data in Figure 6 (curve 2) for $T_s \le 150$ °C. It is interesting to note that the films deposited on unheated substrate were soft, resembling in appearance a polymeric material of low cross-link density.

With increasing T_s the situation alters dramatically. Due to intense cross-linking there will be a substantial drop of the numbers of repeating units n and m in the linear-branched structure produced by reactions 8 and 9. Thermally enhanced surface mobility of adsorbed radicals and vibration of the particular groups in the growing film promote a variety of the heterogeneous (gas–solid) and homogeneous (solid–solid) reactions. The reaction between hydrogen radical and methylsilyl group in carbosilane segments may result in the abstraction of either methyl or hydrogen:

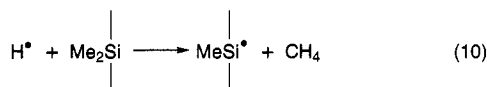

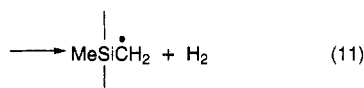

The susceptibility of the Si–Me and C–H bonds in TMSS molecule toward the reaction with atomic hydrogen characterized earlier, allows us to expect reaction 10 to be prevalent. The silyl radicals formed via reaction 10 may abstract hydrogen from the vicinal methyl groups:

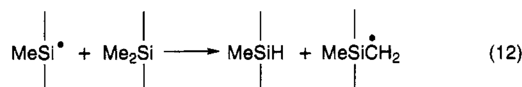

Reaction 12 is confirmed by the appearance in the FTIR spectra (Figure 2b–e) of weak absorption band at 2160 cm^{-1} from SiH_x and increased concentration of these groups as observed from the XPS Si2p data in Figure 5 (curve 1) for $T_s \le 200$ °C.

The radical structure formed in reactions 11 and 12 may readily be converted into silene unit via an endothermic reaction[38,39] involving the elimination of methyl group:

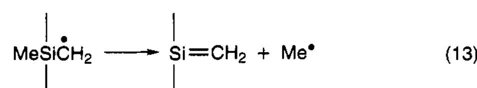

The methyl radicals effusing from the film may react with methylsilyl groups to produce an intermediate radical structure:

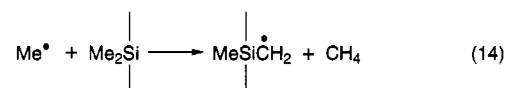

which subsequently undergoes reaction 13. Reactions 10–14 account for a decay of the IR absorption band from the methylsilyl groups in 1260–1240 cm^{-1} region, with rising T_s (Figure 3).

The insertions of silene units formed via reaction 13, to the Si–Me bonds in the vicinal carbosilane segments are considered as the first step of a cross-linking process which may be described by reaction 15:

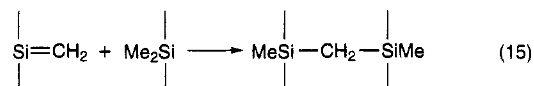

The combination of two vicinal silene units, exothermic in nature[38] and resulting in the formation of four-membered carbosilane ring between the linear segments may also contribute to the cross-linking:

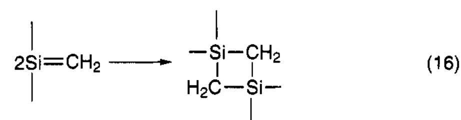

Further steps of cross-linking are involved in the reaction of hydrogen or methyl radicals with carbosilane bond:

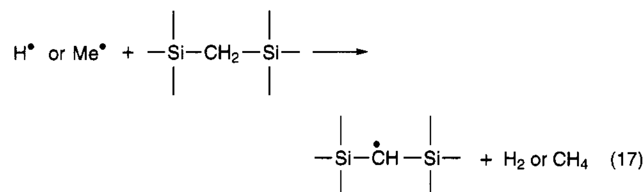

The radical site formed in reaction 17 may combine with the silyl radical from the neighboring segment:

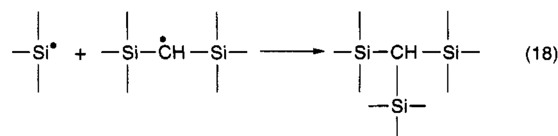

In the next step a similar sequence of the reactions leads to the formation of carbidic network:

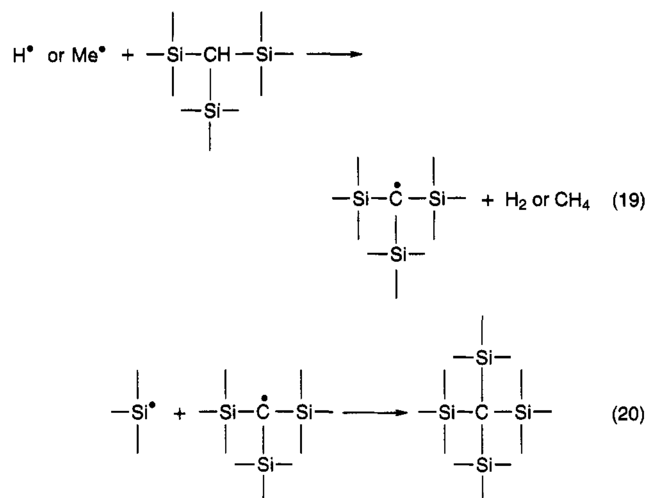

Reactions 17–20 are strongly supported by the evolution of film structure taking place with increasing substrate temperature, as revealed by the following FTIR, XPS, and AES observations:

(i) A marked increase in the intensity of the IR band in 830–800 cm^{-1}, arising from the Si–C carbidic bonds (Figure 3).

(ii) The rise and fall in the intensities of the XPS Si2p peaks (Figure 6) from the Si–C carbidic (curve 2) and $Si-CH_x$ (curve 3) units, respectively. The decreasing intensity of the XPS C1s peak (Figure 7) from the CH_x groups (curve 2) for $T_s \geq 150$ °C.

(iii) The increase of the AES atomic concentration ratio Si/C to the value of stoichiometric silicon carbide (Figure 11).

Properties of the Deposit

Microstructure. In light of distinct changes in the chemical structure of the deposit which are involved in the variation of the substrate temperature, it was interesting to establish the effect of this parameter on the morphology of the film as an important feature determining the quality of the deposited material. Figure 12 presents SEM micrographs of surface of the films deposited on c-Si wafer at various substrate temperatures: 35, 150, 200, and 300 °C. For the contrast, each micrograph was taken from the surface area containing a single particle of the atmospheric dust. As follows from the SEM micrographs in Figure 12, the substrate temperature does not influence the surface morphology of the deposit. The film surface, being very smooth and structureless, exhibits an excellent morphological homogeneity, irrespective of the deposition temperature.

The morphology of the presented film surfaces drastically differs from that of the direct plasma CVD films. The latter materials, and in particular those deposited at low substrate temperature regime, often reveal a morphological heterogeneity manifested by a two-phase structure which comprises spherical or spheroidal powder particles embedded in a continuous film matrix.[42] Although the size of the powder particles essentially does not exceed 1 μm in diameter, their mere presence markedly deteriorates the film's quality in terms of practical properties. The morphology of the direct plasma CVD films produced from organometallic and organosilicon source compounds has been reviewed in ref 42, and according to the discussed literature data the formation of powder particles is associated with a nature of the direct plasma CVD process and resulting initiation of the growth step in the gas phase. The coalescence of the particles which, in turn, start their own growth in the gas phase, is considered to contribute substantially to the process of film formation and growth.

The SEM data in Figure 12, being in contrast with those of the direct plasma CVD films,[42] suggest a homogeneous mechanism for the growth step in the examined remote hydrogen plasma CVD, which seems to proceed exclusively on the substrate.

The reflection high-energy electron diffraction patterns obtained for the films deposited at different substrate temperature in the examined range 30–400 °C, revealed the absence of reflexes which might be assigned to crystalline structure. This accounts for the amorphous structure in the produced films.

Refractive Index. The optical properties of the deposited material are characterized by the refractive index (n) measured ellipsometrically using helium–neon laser light. The measurements were performed for the film samples produced at different substrate temperature. Figure 13 shows the variation of n with the atomic concentration ratio Si/C and/or substrate temperature. The abscissa Si/C and T_s values in this figure are correlated according to the AES data in Figure 11 for the bulk of the film. As follows from the curve in Figure 13 the refractive index rises sharply from 1.5 to 2.4 with increasing atomic ratio Si/C and/or T_s. This trend is presumably due to the densification of the film resulting from a thermally induced cross-linking process which according to the reaction mechanisms presented in the previous section is reflected by the increased Si/C values.

The same character of compositional dependence of the refractive index as shown in Figure 13 is also reported for the a-Si:C:H films produced from SiH_4/CH_4 source mixture by the direct plasma CVD.[43]

Surface Free Energy and Chemical Stability. The surface free energy is a useful parameter which characterizes the physicochemical nature of surface of the deposit and may provide information regarding short-range interaction forces between deposit and other material surfaces in a composite system. Figure 14 shows the dispersive γ_s^d and polar γ_s^p components of the surface free energy of the deposit $\gamma_s = \gamma_s^d + \gamma_s^p$, as a function of the AES atomic concentration ratio Si/C (for the surface region, Figure 11) and/or substrate temperature. As can be noted, γ_s^d varies from about 18 to 37 N m^{-1} with rising ratio Si/C or T_s, whereas γ_s^p remains constant at relatively small value which amounts to 1.7 ± 0.3 N m^{-1}. The observed evolution of γ_s^d can be explained in terms of our earlier finding[44] for the direct plasma CVD films, which reveals that the dispersive

(42) Wróbel, A. M.; Wertheimer, M. R. In *Plasma Deposition, Treatment, and Etching of Polymers*; d'Agostino, R., Ed.; Academic Press: Boston, MA, 1990; Chapter 3.

(43) Catherine, Y.; Turban, G. *Thin Solid Films* **1979**, *60*, 193.

(44) Wróbel, A. M. In *Physicochemical Aspects of Polymer Surfaces*; Mittal, K. L., Ed.; Plenum Press: New York, 1981; pp 197–215.

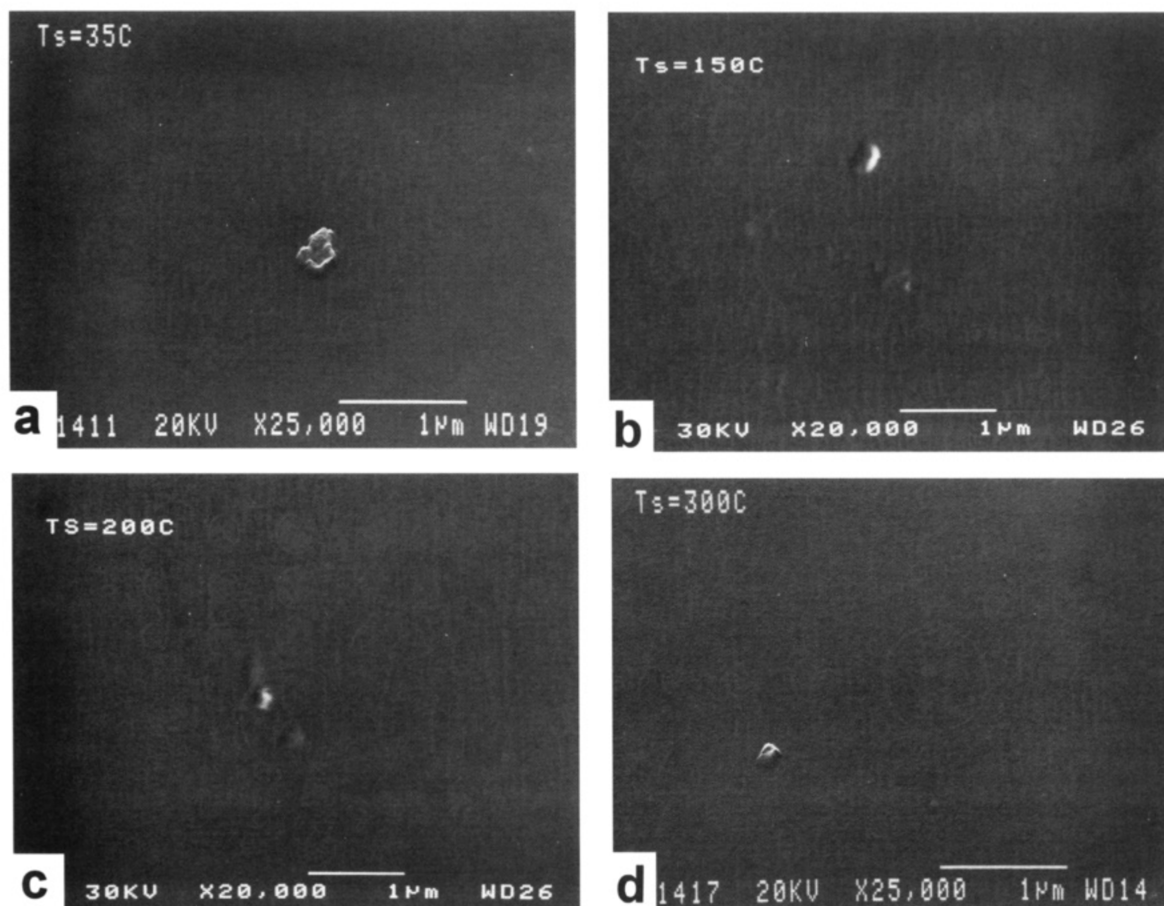

Figure 12. SEM micrographs of the surface of films deposited on c-Si wafer at various substrate temperatures: 35 (a), 150 (b), 200 (c), and 300 °C (d).

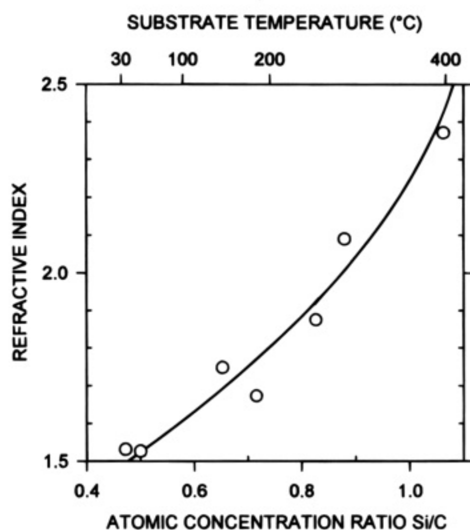

Figure 13. Refractive index at the light wavelength of 632.8 nm, as a function of the AES atomic concentration ratio Si/C and/or substrate temperature.

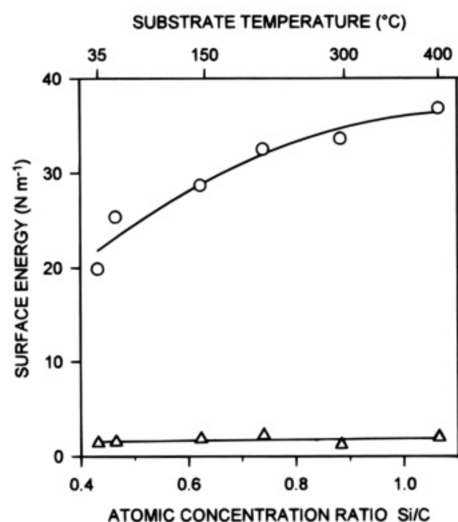

Figure 14. Dispersive (○) and polar (Δ) components of the surface free energy of the film as a function of the AES atomic concentration ratio Si/C (for the surface region) and/or substrate temperature.

component is very sensitive to the cross-link density. Hence, the increase of γ_s^d with rising ratio Si/C or T_s, as follows from Figure 14 is due to the cross-linking process that causes dense packing of structural elements in the film.

On account of the presented data the examined films can be classified as low-surface-energy, and in particular, low-polarity materials.

The films deposited at $T_s \geq 300$ °C exhibited an excellent resistance to acidic media. Long-term treatment (i.e., several days) with hydrochloric, nitric, sulfuric, and chromic acids had no visible effect upon the film surface.

Summary

The present study has proved that deposition temperature in the examined remote hydrogen plasma CVD is the most important parameter, decisive of the structure, compositional uniformity, and properties of the a-Si:C:H film.

The increase in T_s involves the following changes: The organic moieties are eliminated from the film structure which evolves into silicon carbide network. The difference in the stoichiometry between the film surface region and the bulk diminishes and the films produced at $300 \le T_s \le 400$ °C exhibit good compositional uniformity manifested by similar values of the atomic concentration ratio Si/C for the surface region and the bulk.

According to postulated hypothetical reaction mechanisms the film growth takes place by the insertion of dimethylsilene ($Me_2Si{=}CH_2$) formed in the activation step, to the Si−Me bonds in the deposit. An analogous reaction of silene units formed in the deposit is considered to contribute spontaneously to the first step of crosslinking resulting in the formation of carbosilane $Si{-}CH_2{-}Si$ crosslinks. The dehydrogenation of these units at high deposition temperature regime leads to the formation of a carbidic network structure.

The films were found to be amorphous, low-surface-energy and morphologically homogeneous materials. Their refractive index can be controlled by the deposition temperature in a wide range of values, i.e., 1.5−2.4. The materials produced at high substrate temperatures, $T_s \ge 300$ °C, exhibited an excellent resistance to acidic media.

Summarizing, the remote hydrogen plasma CVD seems to be a good technique for the production of homogeneous a-Si:C:H films.

Acknowledgment. This work was financially supported by the Japanese Ministry of Education (Monbusho) . A.M.W. is grateful to the above ministry for granting him a visiting professorship. The authors wish to thank Professor K. Ischikawa for the Raman spectroscopic examination, Mrs Y. Suzuki for performing the XPS analyses, and Professor M. Wysiecki (Technical University of Szczecin, Poland) for his kind assistance in the SEM examination. Special thanks are also addressed to the reviewers for valuable comments. The present study is a part of the KBN research project No. 226859203.

CM9500770